Title: Development of a Fabry-Perot Interferometer for Ultra-Precise Measurements of Column CO_2

Authors: Emily L. Wilson (1), Elena M. Georgieva (2), William S. Heaps (1)

Affiliations: (1) NASA Goddard Space Flight Center
(2) Science Systems and Applications, Inc.

Corresponding Author: Emily L. Wilson
NASA Goddard Space Flight Center,
Laser and Electro-Optics Branch, Code 554
Greenbelt, Maryland 20771, USA
Emily.L.Wilson@NASA.gov

Abstract

A passive Fabry-Perot based instrument is described for detecting column CO_2 through absorption measurements at 1.58μm. In this design, solar flux reaches the instrument platform and is directed through two channels. In the first channel, transmittance fringes from a Fabry-Perot interferometer are aligned with CO_2 absorption lines so that absorption due to CO_2 is primarily detected. The second channel encompasses the same frequency region as the first, but is comparatively more sensitive to changes in the solar flux than absorption due to CO_2. The ratio of these channels is sensitive to changes in the total CO_2 column, but not to changes in solar flux. This inexpensive instrument will offer high precision measurements (error <1%) in a compact package. Design of this instrument and preliminary ground-based measurements of column CO_2 are presented here as well as strategies for deployment on aircraft and satellite platforms.

1. Introduction

Prior to the industrial revolution of the last 250 years, the concentration of carbon dioxide (CO_2) in the atmosphere was 280 ppm, a value that had remained approximately constant (within $\pm$ 10 ppm) for several thousand years (Houghton *et al.*, 2001). When Charles Keeling(Keeling, 1997: Keeling *et al.*, 2004) started measuring atmospheric carbon dioxide from Mauna Loa observatory in 1958, the concentration was on the order 315 ppm.(Keeling, 2005) This value has steadily increased to its current value of 380 ppm.(Keeling, 2005) This recent increase, the rate of which has been unparalleled for the last 20,000 years, is largely due to the anthropogenic emissions of the modern industrial revolution.(Houghton *et al.*, 2001)

The majority of CO_2 variability occurs in the lower atmosphere (~1000 to 800 mbar). Ground-based absorption measurements of the CO_2 column are commonly carried out by Fourier Transform Infrared spectrometry (FT-IR) coupled with a sun tracking system. Typically, these exploited the broad spectral range capable by FT-IR to also include species such as O_2, O_3, CH_4, HCl, N_2, N_2O, HNO_3, HF, and H_2O. Analysis generally involves using an algorithm to fit individual spectral features to reduce noise. Yang, *et al.*(Yang *et al.*, 2002) measured CO_2 at 6300 cm^{-1} and O_2 at 7900 cm^{-1} from the McMath telescope in Kitt Peak, Arizona. The ratio of CO_2 to O_2 is then used to scale to the mean O_2 volume mixing ratio. Precision is estimated at 0.5% after a HITRAN(Rothman, 1998) based spectral fitting routine (JPL) is used to reduce the noise. Goldman, *et al.*(Goldman *et al.*, 1999) compared several FT-IR based instruments (JPL's MKIV, NCAR's Bruker 120 M, and NPL's Bruker 120 M) measuring a variety of trace species including CO_2 from the Jet Propulsion Laboratory's Table Mountain Facility in

Wrightwood, CA and found standard deviations from the mean column to range from 0.5 to 2% for CO_2.

While these FT-IR techniques offer good sensitivities, cost and size limit the viability for this method fill in the sparse spatial network of surface measurements and ultimately resolve major source and sink regions. Conversely, while space-based measurements of this greenhouse gas offer good spatial coverage as well as temporal resolution, historically, they have not offered adequate precision for resolving key sources and sinks.(O'Brien and Rayner, 2002: Sarmiento and Gruber, 2002) Transport inversion model experiments indicate global column measurements with an uncertainty of 2.5 ppm or better (<1%) would greatly improve surface flux estimates(Pak and Prather, 2001: Rayner and O'Brien, 2001)

In this article, we present an application of a Fabry-Perot interferometer for measurements of spectral absorption of sunlight by CO_2. Since its inception in 1899, Fabry-Perot interferometers have found wide applications as background filters in atmospheric research. Mack, *et al.*(Mack *et al.*, 1963) described the PEPSIOS™ (polyetalon pressure-scanned interferometric optical spectrometer) that used several Fabry-Perot etalons to isolate a spectral bandpass. With each etalon in its own pressure chamber, scanning the etalon was accomplished by varying the pressure of the inert gas between the etalon plates, and thus varying the refractive index of the inert gas. Larar et al.(Larar *et al.*, 1998) proposed a double-etalon Fabry-Perot interferometer as a nadir-viewing satellite instrument for global tropospheric and total ozone monitoring at 9.6 μm. In the accompanying feasibility study, Larar and Drayson(Larar and Drayson, 1998) predict precisions of 12% and 3.6% respectively. In addition, a retrieval method using a

nonlinear least-squares iterative technique to achieve convergence of the measured and calculated forward model signals is described. Skinner, *et al.*(Skinner *et al.*, 1987) investigated a triple etalon Fabry-Perot interferometer for measuring Doppler shifts of rotational lines of O_2 in the atmosphere from the Upper Atmosphere Research Satellite as a means for determining wind vectors in the stratosphere and mesosphere. Finally, McKay(McKay, 1999) compares the application of single, double and triple Fabry-Perot etalon pairs as solar background filters in lidar. Tunable air-gap etalons are aligned to lidar signal spectrum to reduce signal interference caused by the scattering of sunlight into the field of view. Reflective coupling between etalons was found to limit potential contributions of second and third etalons.

The instrument presented here offers a smaller, less expensive, and mechanically less-complex alternative to FT-IR techniques with equal sensitivity. Additionally, this technique can be packaged to shoe-box size for use in either ground-based applications or deployment on an aircraft or satellite platform. We have assembled a laboratory prototype system and have conducted validation experiments in the lab as well as measured CO_2 in the atmosphere in ground measurements using both direct sunlight, and sunlight reflected off of a Lambertian surface. Preliminary results indicate that the method will be able to achieve the sensitivity and signal-to-noise detection required to measure column CO_2 at the target specification. In addition, we have begun development of a similar instrument for measuring O_2 to correct for temperature fluctuations as well as changes in surface pressure. Methods for increasing sensitivity and stability of the instrument will also be addressed.

2. Instrument Design

The instrument described here employs a Fabry-Perot Interferometer to measure the carbon dioxide column through absorption of sunlight at 1.58μm. In this design, sunlight passes through the atmosphere where it undergoes some absorption by atmospheric carbon dioxide. The light is then introduced into the instrument and split into two channels. The first channel simply measures the total light intensity. This channel responds to changes in overall intensity arising from changes in atmospheric transmission, changes in atmospheric CO_2, and when viewing surface reflected light, changes in ground albedo. The second channel is identical to the first except that it includes a solid etalon Fabry-Perot interferometer tuned to pass light at the wavelengths that CO_2 absorbs and reflect light at other wavelengths. This channel responds to albedo and atmospheric transmission changes just as the first channel but proportionately much more strongly to changes caused by changing CO_2. The ratio of the signals of the two channels can be used to infer the atmospheric CO_2 abundance. A schematic of this instrument is shown in **Figure 1**.

In this design, an off-axis parabolic mirror (OAP) focuses incoming light onto a 2 mm diameter aperture to restrict the field of view of the instrument. Following the aperture, the light is modulated at 400 Hz with a chopper (Stanford Research Systems, SR540). Chopped light is then re-collimated with a second OAP and passes through a 1567-1574 nm bandpass filter (Barr Associates). Approximately 10% of of this light is split with a (fused Si) beamsplitter (CVI), and focused onto the first of two thermo-electric cooled InGaAs photodiode detectors (Oriel Instruments). This first (reference) channel monitors changes in solar flux.

Light passing through the beam splitter continues through a solid Fabry-Perot interferometer (CVI), and is focused onto the second InGaAs detector forming the Fabry-Perot channel. Both the prefilter and Fabry-Perot interferometer optics are mounted in ovens (Andover) and temperature controlled to 1/100th degree. Both Fabry-Perot and Reference signals are processed through lock-in amplifiers (Stanford Research Systems, SR830 DSP) referenced to the frequency of the chopped signals. Custom LabVIEW software (National Instruments, version 6.1) has been developed for controlling the measurement system as well as analyzing the detected signals from both channels. The ratio of these signals can then be related to changes in the CO_2 column.

A. Fabry-Perot Characteristics

The Fabry-Perot in this instrument is solid fused silica with a free spectral range (FSR) of 0.306 nm, a refractive index of 1.443 at λ=1571 nm, and a clear aperture of 50 mm. The interference produced by a Fabry-Perot Interferometer (**Figure 2**) can be described by the Airy function (Born and Wolf, 1999: Ingle and Crouch, 1988):

$$\frac{\Phi}{\Phi_m} = \frac{1}{1 + C_F \sin^2\left(\frac{\delta}{2}\right)} \qquad (1)$$

where Φ/Φ_m is the fractional radiant power, C_F is the coefficient of finesse, and δ is the phase difference between the interfering waves. The finesse (F) of the etalon is related to the reflectance (R) of its surfaces as shown in the following equation. Also detailed are the free spectral range (FSR) and full width at half maximum (FWHM) of the interference fringes.

$$F = \frac{FSR}{FWHM} = \frac{\pi\sqrt{R}}{1-R} = \frac{\pi\sqrt{C_F}}{2} \quad (2)$$

The free spectral range is the distance between these interference fringes, determined by the wavelength (λ) of the interfering light, the thickness of the etalon (d) and the refractive index (n) of the etalon material where the FSR, λ, and d are in units of nm:

$$FSR = \frac{\lambda^2}{2nd} \quad (3)$$

Thus, the spacing between fringes can be approximately matched to the spacing of CO_2 lines through etalon thickness. Similarly, the width of fringes can be approximately matched to CO_2 line width by appropriate choice of reflectance of the etalon surfaces.

B. Etalon Temperature Tuning

Alignment between fringes and CO_2 absorption transitions can be further adjusted by temperature tuning the Fabry-Perot. As the temperature changes, the refractive index of a Fabry-Perot optical medium changes as:

$$\mu = \mu_0 + \beta(T - T_0) \quad (4)$$

where μ_0 is the refractive index at temperature T_0, and β is the refractive index change coefficient. With increasing temperature, etalon fringes shift to longer wavelengths by typically 0.02 nm per °C for fused silica.(Slyusarev, 1984)

Alignment between fringes and CO_2 lines at two different temperatures is demonstrated in **Figure 3(a),** where two laser scans of carbon dioxide (1 atm) in an absorption cell are obtained with the instrument etalon at temperatures of 42° and 54°C. Fringes from the Fabry-Perot channel shown in light and dark gray respectively are

compared with CO_2 lines from the reference channel in black. Fringes and rotational features are shown with the bandpass prefilter defining the wavelength range of the instrument. The 54°C scan clearly shows better overlap between fringes and lines than the 42°C scan. To validate in the laboratory that improved overlap corresponds with greater instrument sensitivity, changes in the ratio of Fabry-Perot to Reference signals were monitored for CO_2 pressures ranging from 0 to 1000 torr in a 1.4 m absorption cell at both Fabry-Perot temperatures. Laboratory measurements using a 1.4 meter absorption cell at 1000 Torr are comparable to a column absorption of approximately ¾ that of the true atmospheric column. Results for this experiment are shown in **Figure 3(b)** where the ratio of Fabry-Perot/Reference signals decrease as the pressure in the gas cell increase. While some change in the ratio is seen with poor overlap (42°C), at Fabry-Perot temperatures where there is good overlap (54°C), the ratio is considerably more sensitive to changes in CO_2 pressure.

3. Ground Testing

The Fabry-Perot instrument has two potential modes of operation; one as a ground based sensor, and one as an aircraft or satellite deployable instrument. In the first configuration, the CO_2 column is measured through absorption of light by CO_2 in the atmosphere directly between the sun and the ground instrument. We accomplished this by collecting light with a small telescope fixed to an equatorial mount, aligned to track the sun throughout the day. An optical fiber coupled at the rear of the collimator brings light into the instrument. In the second configuration, light passing through the atmosphere reflects on the Earth's surface before entering the instrument platform. This is the way the

instrument would be used for remote sensing of the CO_2 column from an airborne or spaceborne platform. We have tested the instrument's performance in this mode simply by introducing light reflected off the ground. The flux entering the instrument is independent of its height above the ground because the area included in its field of view increases at the same rate as its overall collection efficiency decreases. While this approach should be more sensitive to changes in CO_2 because the light passes through the atmosphere twice before entering the instrument, the retrieval of the actual CO_2 column from the measurement is complicated by scattering effects in the atmosphere.

A. Sun tracker results

In general, the ratio arising from direct illumination should depend upon the path length through the atmosphere (airmass) regardless of changes in cloud and aerosol distribution. The ratio then should follow Beer's law in the form:

$$R_{calc} = R_o + I_o e^{-k(Airmass)} \tag{5}$$

for modest values of airmass, where airmass is estimated by

$$Airmass = \sec\left(2/\pi - ALT\right) \tag{6}$$

and ALT is the solar altitude in radians.(U.S._Naval_Observatory, 2003) It should however be noted that this formula assumes that there is no saturation by the absorber. Ground measurement of the CO_2 column made from Edwards, CA on May 13, 2004 are shown in **Figure 4**. The ratio of Fabry-Perot to Reference signals (filled circles) clearly follows changes in the airmass throughout the day.

To validate that changes in the ratio signal were indeed due to changes in the CO_2 column, outdoor experiments were conducted in which a 1.4 m absorption cell was

aligned at the front of the instrument, and CO_2 pressures in the cell were varied from 0 to 1000 torr. Experiments were conducted at midday when changes in the airmass were minimal. The results of these trials are shown in **Figure 5**, where the ratio of Fabry-Perot to reference signals are shown as a function of total CO_2 measured in the cell and column. In this Figure, it was assumed that 1 torr of CO_2 in the cell is equivalent to 0.263 ppm of CO_2 in the column. This experiment also serves to calibrate the observed ratio to the total CO_2 measured. However, this is only useful in the linear region of this figure extending to approximately 600 ppm. Beyond this, the affects of self-broadening of CO_2 in the absorption cell become evident.

B. Reflected flux measurements

Preliminary tests of the instrument in the reflected light viewing mode were also carried out on the ground by having the instrument view a Lambertian surface (Spectralon) at ground level with a downward viewing mirror approximately a meter above the surface. Radiation incident on a surface is partially direct and partially diffuse. The direct component of this radiation is a result of the direct solar beam passing through the atmosphere while the diffuse component is a result of atmospheric scattering. For a clear sky condition, the direct component is about 80% of total incident solar radiation in visible and infrared regions.(Qin *et al.*, 2001) We estimate the direct component of sunlight by measuring total intensity and then blocking the sunlight over the region observed by the instrument to infer the indirect illumination.

Figure 6 shows ground data taken in this method in July 2005. Data for both days are shown with 15 second averaging. The general form of the ratio signal reflects

changes in the airmass throughout the day. Noisier regions show increased cloud cover in the morning of July 20, and after 3:00 p.m. (15) on July 21, as well as low signal levels in morning and evening. The signal spikes (seen at 30 minute intervals) show the change in ratio when the direct light is blocked and only indirect (scattered) light reaches the instrument. The direction that spikes point depends on whether the scattered light travels a longer path (decreases ratio) or shorter path (increases ratio) through the column than the direct light.

An illustration of this is shown in **Figure 7**. For the high sun example at left, the scattered light has a longer absorption pathlength through the column than the direct light. With low sun (at right), the absorption pathlength of the scattered light is shorter than that of the direct light because there is very little CO_2 along the high altitude path through the atmosphere before the scatter occurs. While blocking the direct light results in an increase in the ratio for data taken on this date, data taken on other dates have shown the ratio to decrease with blocking when the sun is low in the sky. This effect is complicated by varying cloud heights, aerosols, altitude variability of the CO_2, etc. and poses a significant retrieval challenge.

C. Sensitivity and Noise Estimate

In both sun tracker and reflected flux measurements, changes in the CO_2 ratio were found to track changes in the airmass throughout the day. This temporal correlation was exploited to produce the calibration curve shown in **Figure 8(a)** where changes in the CO_2 ratio are plotted as a function of airmass. For this plot, ground data acquired with the sun tracker were used (See **Figure 4**). It can be seen that the ratio changes by ~0.10

for an approximate airmass change of 4 (about 0.025 for an airmass change of 1). One airmass is approximately equal to 360 ppm of CO_2. Thus, the sensitivity of the ratio to a 1 ppm change in CO_2 is 0.025/360 = 0.000069.

An expansion of the noise in this calibration curve taken at 1/10 second intervals is shown in **Figure 8(b)**, with the ten point average shown as a solid line. The standard deviation in noise for data taken at 1/10 second intervals is $\pm$ 0.00025. In one second, the mean error is equal to $0.00025/\sqrt{10} = 0.000079$. If the detection limit is defined as a 2:1 SNR, twice the noise is 0.000079 x 2 = 0.00016, then the current instrument detection limit is 0.00016 x 1 ppm/0.000069 = 2.3 ppm in a one second average. This implies the ground based instrument performance would be better than the desired sensitivity of 1 ppm in less than ten seconds of averaging.

4. Conclusions and Future Directions

Presented here is a prototype design for a passive Fabry-Perot based instrument to make absorption measurements of total column carbon dioxide using sunlight at 1.58μm. This instrument has been demonstrated as a ground based sensor when used in conjunction with a positioning system to follow sun movement. Signals from these data trials were found to consistently track changes in airmass. Additionally, laboratory experiments validate the instrument's sensitivity to changes in CO_2. An estimate of the system performance indicates that this design has the capability to resolve changes in the CO_2 column as small as 2.3 ppm with a one second average and better than 1 ppm in less than 10 seconds averaging.

Preliminary ground data have also been presented using surface reflectance to measure the CO_2 column. While this second configuration is a clear lead to deployment of the Fabry-Perot instrument on an airborne platform, it also presents some additional retrieval challenges due to contributions of aerosol scattering in the reflected signal. While contributions from aerosol scattering can be measured and easily corrected during ground measurements using surface reflectance, deconvolution of scattering in airborne measurements poses a far greater challenge. This clearly will also be an issue for other passive instruments measuring absorption of the CO_2 column as well as other trace gases.

Acknowledgments

This research was funded by the NASA Earth Sun-System Technology Office (ESTO) Instrument Incubator Program (IIP).

References

Born, M. and E. Wolf, 1999: *Principles of Optics*. 7th ed. Cambridge University Press, 360-371 pp.

Goldman, A., C. Paton-Walsh, W. Bell, G. C. Toon, J.-F. Blavier, B. Sen, M. T. Coffey, J. W. Hannigan, and W. G. Mankin, 1999: Network for the Detection of Stratospheric Change Fourier transform infrared intercomparison at Table Mountain Facility, November 1996. *J. Geophys. Res.*, **104,** 30481-30503.

Houghton, J. T., Y. Ding, D. J. Griggs, M. Noguer, P. J. van der Linden, and D. Xiaosu, 2001: Climate Change 2001: The Scientific Basis.

Ingle, J. D. and S. R. Crouch, 1988: *Spectrochemical Analysis*. Prentice-Hall, Inc., 590 pp.

Keeling, C. D., 1997: Climate change and carbon dioxide: An introduction. *Proc. Natl. Acad. Sci. USA*, **94,** 8273-8274.

Keeling, C. D., 2005: Atmospheric CO_2 concentrations (ppmv) derived from in situ air samples collected at Mauna Loa Observatory, Hawaii.

Keeling, C. D., H. Brix, and N. Gruber, 2004: Seasonal and long-term dynamics of the upper ocean carbon cycle at Station ALOHA near Hawaii. *Global Biogeochem. Cycles*, **18,** Art. no. GB4006.

Larar, A. M. and S. R. Drayson, 1998: Global tropospheric and total ozone monitoring with a double-etalon Fabry-Perot interferometer II. Feasibility analysis. *Applied Optics*, **37,** 4732-4743.

Larar, A. M., P. B. Hays, and S. R. Drayson, 1998: Global tropospheric and total ozone monitoring with a double-etalon Fabry-Perot interferometer. I. Instrument concept. *Applied Optics*, **37,** 4721-4731.

Mack, J. E., D. P. McNutt, F. L. Roesler, and R. Chabbal, 1963: The PEPSIOS Purely Interferometric High-Resolution Scanning Spectrometer. I. The Pilot Model. *Applied Optics*, **2**.

McKay, J. A., 1999: Single and tandem Fabry-Perot etalons as solar background filters for lidar. *Applied Optics*, **38,** 5851-5858.

O'Brien, D. M. and P. J. Rayner, 2002: Global observations of the carbon budget 2. CO_2 column from differential absorption of reflected sunlight in the 1.61 mm band of CO2. *Journal of Geophysical Research*, **107,** 4354.

Pak, B. C. and M. J. Prather, 2001: CO_2 source inversions using satellite observations of the upper troposphere. *Geophys. Res. Lett.*, **28,** 4571-4574.

Qin, W., J. Herman, and Z. Ahmad, 2001: A fast, accurate algorithm to account for non-Lambertian surface effects on TOA radiance. *J. Geophys. Res.*, **106,** 22671-22684.

Rayner, P. J. and D. M. O'Brien, 2001: The utility of remotely sensed CO_2 concentration data in surface source inversions. *Geophys. Res. Lett.*, **28,** 175-178.

Rothman, L. S. e. a., 1998: The HITRAN Molecular Spectroscopic Database and HAWKS (HITRAN Atmospheric Workstation): 1996 edition. *J. Quant. Spectros. Radiat. Transfer*, **60,** 665-710.

Sarmiento, J. L. and N. Gruber, 2002: Sinks for Anthropogenic Carbon. *Physics Today*, 30-36.

Skinner, W. R., P. B. Hays, and V. J. Abreu, 1987: Optimization of a triple etalon interferometer. *Applied Optics*, **26,** 2817-2827.

Slyusarev, G., 1984: *Aberation and Optical Design Theory*. Adam Hilger, Ltd.

U.S._Naval_Observatory, 2003: Astronomical Applications Department.

Yang, Z., G. C. Toon, J. S. Margolis, and P. O. Wennberg, 2002: Atmospheric CO2 retrieved from ground-based near IR solar spectra. *Geophys. Res. Lett.*, **29,** 1339-1343.

Figure Captions

Figure 1. Optical and electronic schematic for Fabry-Perot instrument. Incoming light is divided into Fabry-Perot (detector 2), and reference (detector 1) channels, measuring changes in CO_2 absorption and solar flux, respectively. The ratio of these signals can then be related to changes in the CO_2 column.

Figure 2. Interference in a Fabry-Perot Interferometer. The full width at half maximum (FWHM) and free spectral range (FSR) are indicated by arrows.

Figure 3. In (a), fringe – CO_2 line overlap is compared at two Fabry-Perot temperatures. In (b), the change in ratio as a function of CO_2 pressure in an absorption cell is compared for good (54°C) and poor (42°C) fringe-line overlap.

Figure 4. Ground measurement of the CO_2 column on May 13, 2004. In this configuration, light enters the instrument via a fiber-coupled collimator on an equatorial mount, which tracks sun throughout the day. The ratio (Fabry-Perot/Reference) signal (filled circles) clearly follows changes in the airmass (dashed line).

Figure 5. Field testing instrument validation at mid-day. CO_2 pressure in a 1.4 m absorption cell placed in front of the instrument ranged from 0 to 1000 torr. The ratio of Fabry-Perot to Reference signals is plotted as a function of total CO_2 observed.

Figure 6. Ground data taken with sun light reflected on a Lambertian surface. Direct light hitting this surface is blocked every 30 minutes to illustrate the contribution of scattered light to the signal.

Figure 7. Contribution of scattered light to the ratio. With the sun in a higher position (left), the optical pathlength of the scattered light may be longer than that for the direct

sunlight's path. If the sun is lower in the sky (right), the scattered light may travel a shorter path through the column.

Figure 8. In **(a),** the CO_2 ratio from ground measurements on May 13, 2004 is calibrated to the airmass. Enlargements of noise for data taken at 1/10 second is shown in **(b)** with a ten point average shown as a solid line.

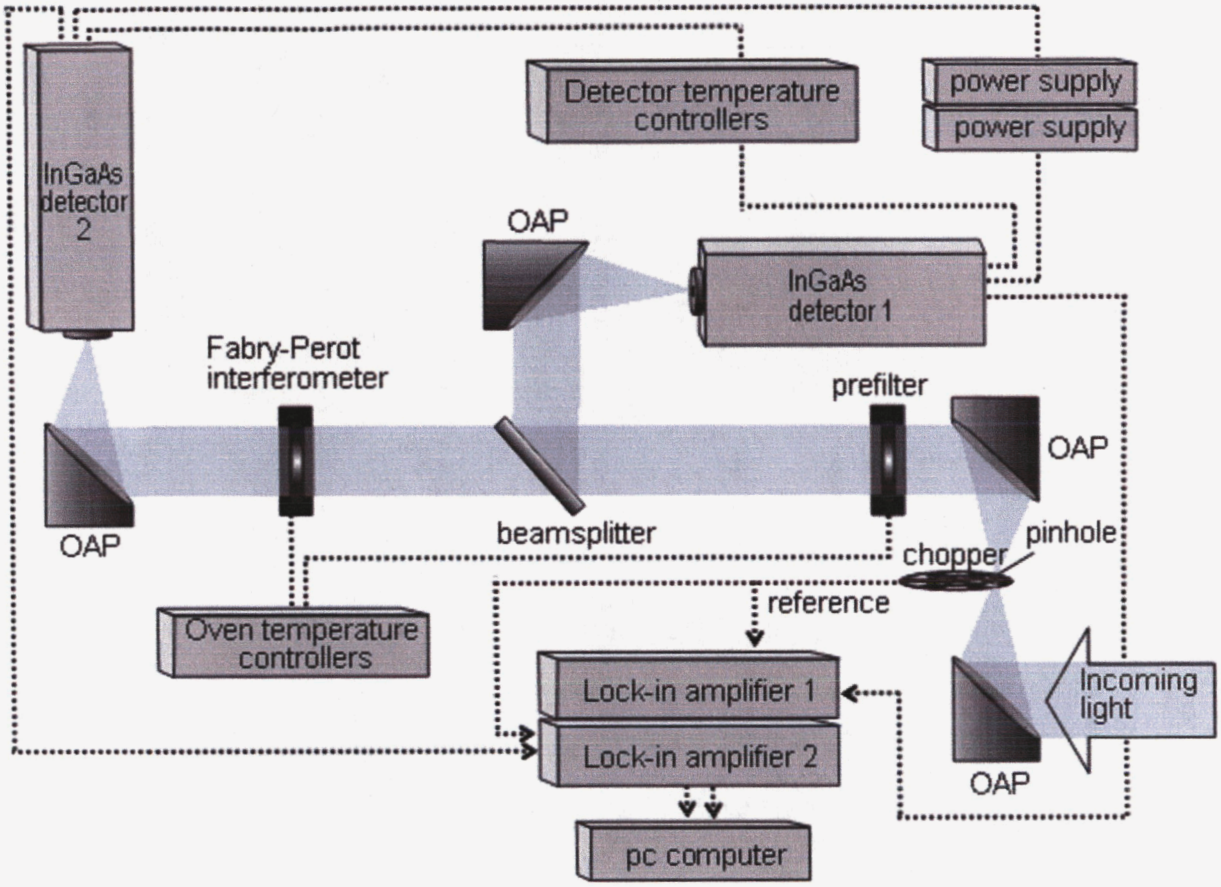

Figure 1. Optical and electronic schematic for Fabry-Perot instrument. Incoming light is divided into Fabry-Perot (detector 2), and reference (detector 1) channels, measuring changes in CO_2 absorption and solar flux, respectively. The ratio of these signals can then be related to changes in the CO_2 column.

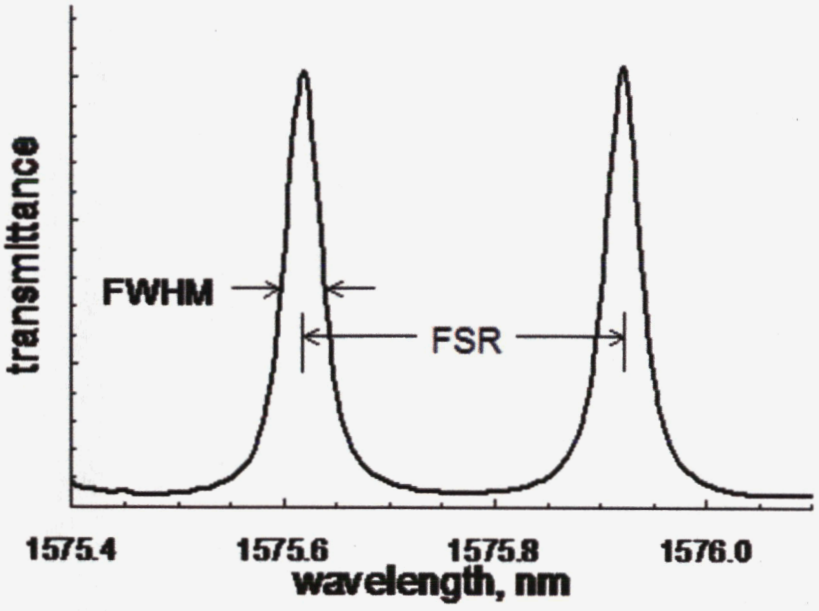

Figure 2. Interference in a Fabry-Perot Interferometer. The full width at half maximum (FWHM) and free spectral range (FSR) are indicated by arrows.

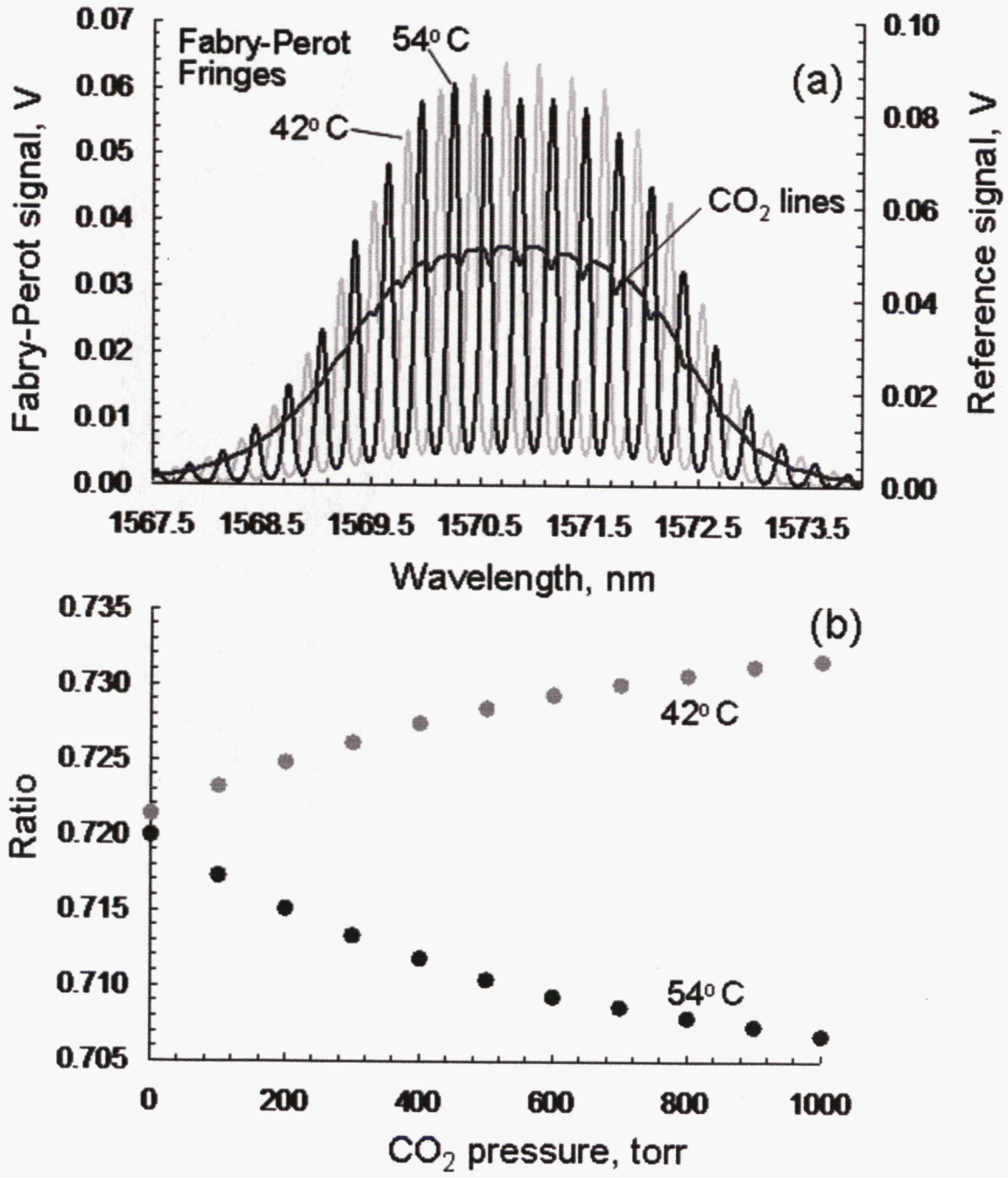

Figure 3. In (a), fringe – CO_2 line overlap is compared at two Fabry-Perot temperatures. In (b), the change in ratio as a function of CO_2 pressure in an absorption cell is compared for good (54°C) and poor (42°C) fringe-line overlap.

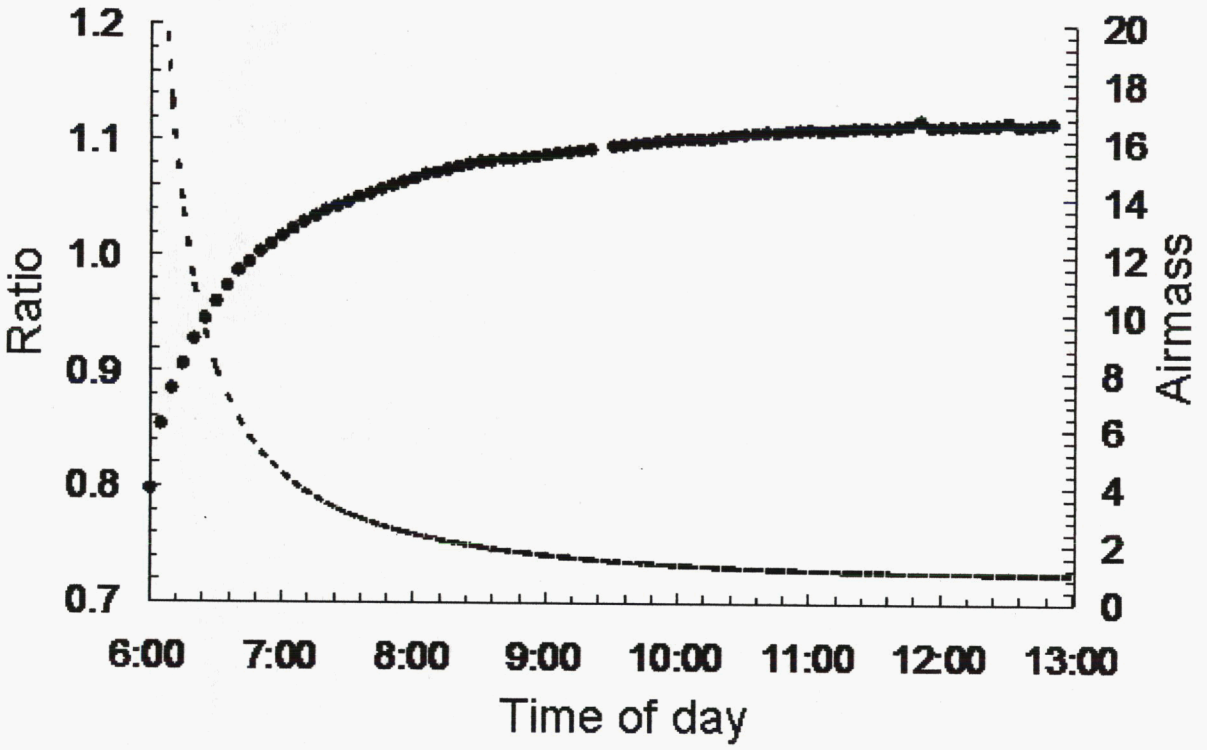

Figure 4. Ground measurement of the CO_2 column on May 13, 2004. In this configuration, light enters the instrument via a fiber-coupled collimator on an equatorial mount, which tracks sun throughout the day. The ratio (Fabry-Perot/Reference) signal (filled circles) clearly follows changes in the airmass (dashed line).

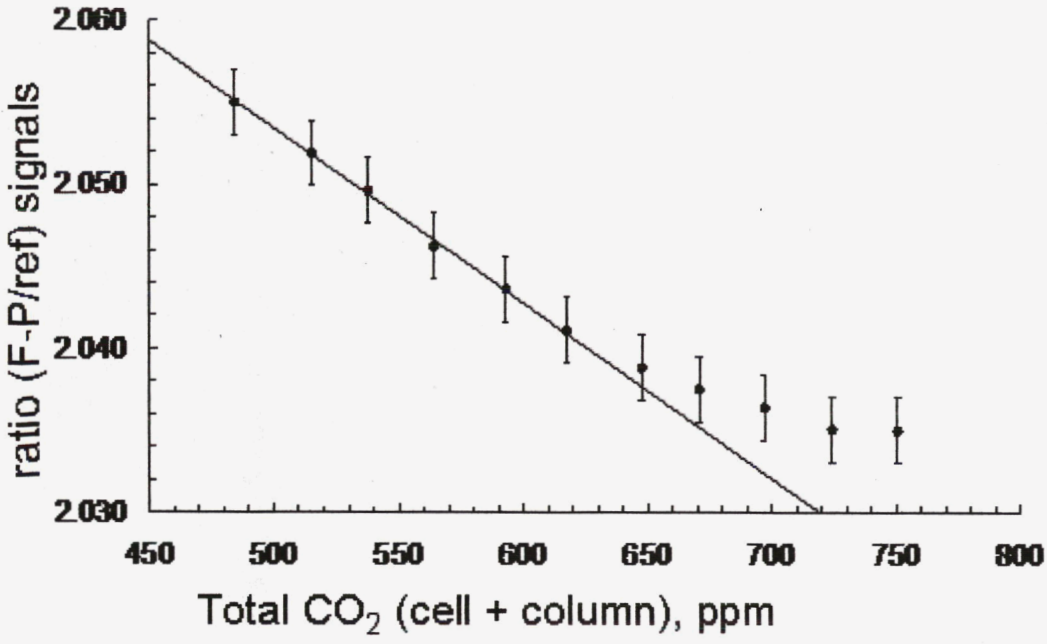

Figure 5. Field testing instrument validation at mid-day. CO_2 pressure in a 1.4 m absorption cell placed in front of the instrument ranged from 0 to 1000 torr. The ratio of Fabry-Perot to Reference signals is plotted as a function of total CO_2 observed.

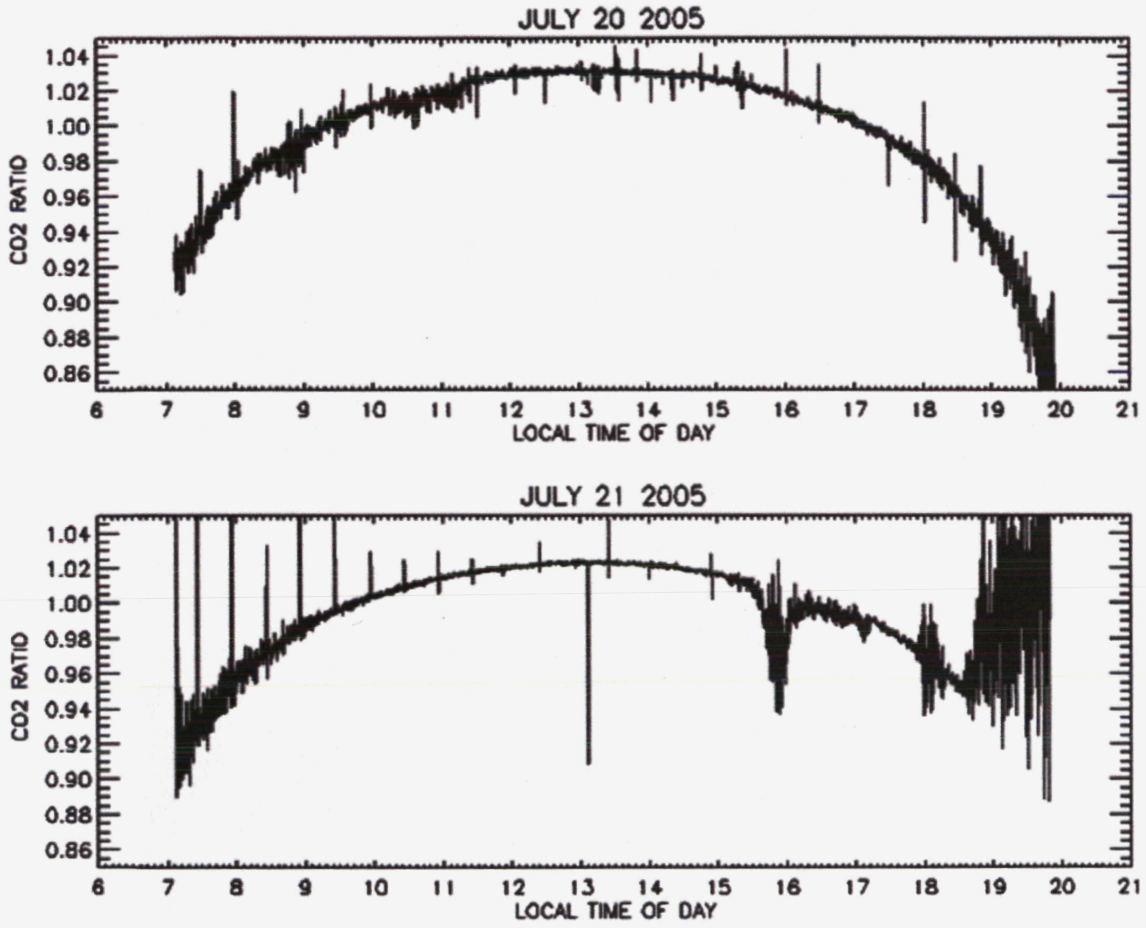

Figure 6. Ground data taken with sun light reflected on a Lambertian surface. Direct light hitting this surface is blocked every 30 minutes to illustrate the contribution of scattered light to the signal.

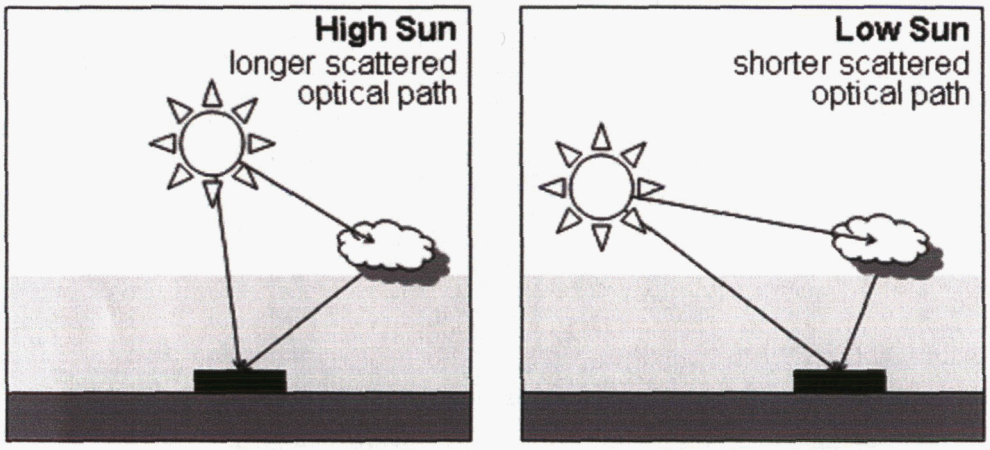

Figure 7. Contribution of scattered light to the ratio. With the sun in a higher position (left), the optical pathlength of the scattered light may be longer than that for the direct sunlight's path. If the sun is lower in the sky (right), the scattered light may travel a shorter path through the column.

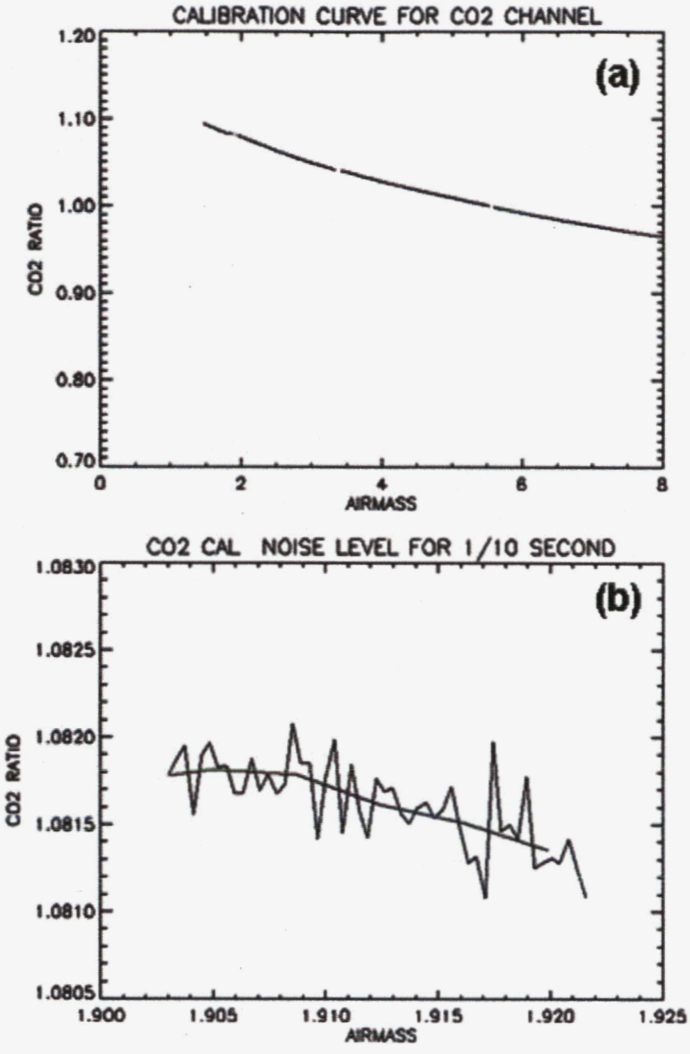

Figure 8. In **(a)**, the CO_2 ratio from ground measurements on May 13, 2004 is calibrated to the airmass. Enlargements of noise for data taken at 1/10 second is shown in **(b)** with a ten point average shown as a solid line.